Supplementary Material for

Nucleoside diphosphate kinases fuel dynamin superfamily proteins with GTP for membrane remodeling

Mathieu Boissan,* Guillaume Montagnac,† Qinfang Shen, Lorena Griparic, Jérôme Guitton, Maryse Romao, Nathalie Sauvonnet, Thibault Lagache, Ioan Lascu, Graça Raposo, Céline Desbourdes, Uwe Schlattner, Marie-Lise Lacombe, Simona Polo, Alexander M. van der Bliek, Aurélien Roux, Philippe Chavrier*

*Corresponding author. E-mail: mathieu.boissan@inserm.fr (M.B.); philippe.chavrier@curie.fr (P.C.)

Published 27 June 2014, *Science* **344**, 1510 (2014)
DOI: 10.1126/science.1253768

This PDF file includes:

Other Supplementary Material for this manuscript includes the following:
(available at www.sciencemag.org/content/344/6191/1510/suppl/DC1)

Movies S1 to S3

Materials and Methods

Cell culture

Human HeLa cells (a gift from A. Dautry-Varsat, Institut Pasteur, Paris, France), Hep2 cells stably expressing interleukin-2 receptor β subunit (*22*) and african green monkey kidney epithelial BSC-1 cells (ATCC CCL-26) were grown in DMEM supplemented with 10% fetal calf serum, 2 mM glutamine and 150 μg/mL penicillin/streptomycin at 37°C in 5% CO_2.

Reagents

Alexa-488-conjugated human Tf, Alexa-488- and Alexa-647-conjugated human EGF were purchased from Molecular Probes (Interchim). Tf-Biotin conjugates were from Life Technologies. Protein-A gold conjugates were purchased from Cell Microscopy Center, Utrecht, Netherlands. The following lipids were purchased from Avanti Polar Lipids, Inc (Alabaster, AL): brain polar lipids preparation (BPL), phosphatidylinositol-4,5-bisphosphate (PtdIns (4,5) P_2), 1-palmitoyl-2-oleoyl-*sn*-glycero-3-phosphocholine (POPC), 1-palmitoyl-2-oleoyl-*sn*-glycero-3-phosphoethanolamine (POPE), 1',3'-bis(1,2-dioleoyl-sn-glycero-3-phospho)-*sn*-glycerol (cardiolipin). Lipid vesicles composition was designed to mimic the lipid composition of plasma membrane or mitochondrial inner membrane. The lipid compositions of the liposomes, by percent-weight, were as follows: plasma membrane mix, 95% BPL, 5% PtdIns (4,5) P_2; mitochondria inner membrane mix, 45% POPC, 22% POPE, 8% PtdIns (4,5) P_2, 25% cardiolipin. GTP and ATP were purchased from Roche Diagnostics (Mannheim, Germany). GDP was purchased from Sigma-Aldrich (St. Louis, MO). Mitochondrion-selective dye MitoTracker™ Red CMXRos was purchased from Molecular Probes.

Antibodies

Selective rabbit polyclonal anti-NM23-H1 and anti-NM23-H2 antibodies were previously described (*23*). Rabbit polyclonal pan-NM23 antibodies (recognizing both NM23-H1 and -H2 isoforms) were prepared by affinity purification using purified human recombinant NM23-H1 and -H2 proteins coupled to NHS-activated HiTrap columns. Mouse monoclonal anti-NM23-H2 was purchased from Kamiya Biomedical Company (Seattle, WA). Polyclonal anti-human NM23-H4 antibodies have been previously described (*14*). Mouse monoclonal anti-RhoA antibody (clone 26C4) was a gift from J. Bertoglio (Institut Gustave Roussy, Villejuif, France). Mouse monoclonal anti-α-tubulin (clone DM 1A) was purchased from Sigma-Aldrich (St. Louis, MO). Mouse monoclonal anti-transferrin receptor antibody (clone H 68.4) was obtained from Zymed Laboratories Inc. (South San Francisco, CA). Polyclonal anti-dynamin-2 antibodies used for Western blotting analysis and mouse monoclonal anti-α-adaptin antibody (clone AC1-M11) were obtained from Abcam (Cambridge, MA, USA). Polyclonal anti-dynamin-2 antibodies (immunofluorescence and PLA experiments) were a kind gift of Dr. P. De Camilli (Yale University School of Medicine, New Haven, CT). Mouse monoclonal anti-dynamin-1 was from Cell Signaling Technology Inc (Beverly, MA). Mouse monoclonal antibody against OPA1 was purchased from BD Biosciences (Le Pont-De-Claix, France). Polyclonal anti-α-adaptin (M-300) and anti-RhoGDIα (A-20) antibodies were purchased from Santa Cruz Biotechnology Inc. (Santa Cruz, CA). Mouse monoclonal anti-caveolin-

2 and anti-clathrin heavy chain antibodies were purchased from BD Biosciences (Le Pont-De-Claix, France).

Protein purification

Human recombinant NM23-H1 wild-type (NM23-H1^{wt}) and catalytically-inactive (NM23-H1^{H118N}) proteins were purified as described previously (*24*). Human recombinant NM23-H2 was produced with the following modifications: the enzyme was eluted from a Blue-Sepharose column by 1mM ATP at pH 8.0. Like NM23-H1 proteins, NM23-H2 was purified by size-exclusion chromatography on a Sephacryl S-200 column. Bacterial expression and purification of NM23-H4 has been described elsewhere (*14*).
Rat dynamin was purified from rat brain using the GST-tagged SH3 domain of rat amphiphysin-2 as an affinity ligand as described (*6*). Recombinant human dynamin-1 and dynamin-2 were purified in a nucleotide-free state from Sf9 cells infected with recombinant baculovirus using the BD BaculoGold^{TM} expressing system (BD Biosciences, Franklin Lakes, NJ, USA) using GST-tagged SH3 domain of rat amphiphysin-1 (*7*). Purified recombinant OPA1 was a kind gift of Dr. J.E. Hinshaw (NIH-NIDDK, Bethesda) (*25*). Dynamin-2 GST-PRD construct kindly provided by Dr. P. De Camilli (Yale University School of Medicine, New Haven, CT) was transformed in *Escherichia coli* BL21 (DE3) strain and the protein was produced and purified according standard procedures.

DNA constructs and transfection

cDNA encoding wild-type NM23-H1^{wt} or catalytically-inactive NM23-H1^{H118N} mutant were cloned in pcDNA3 expression vector. Sequences and mutation were verified by nucleotide sequencing. The pd2EGFP-N1 vector (Clonetech) was used to express the full-length NM23-H3 protein fused to the N terminus of the green fluorescent protein (GFP). The cDNA was generated by polymerase chain reaction using primers that contained BamHI and EcoRI sites and the pJC20 NM23-H3 vector as a template (*26*). The amplified DNA fragment was cloned into the BamHI-EcoRI sites of the pd2EGFP-N1 plasmid.
HeLa cells were transfected with FUGENE reagent according to the manufacturer's instructions (Roche Diagnostics, Mannheim, Germany) and analyzed 24 hours post-transfection. BSC-1 cells were transfected with Lipofectamine reagent according to the manufacturer's procedure (Invitrogen Life Technologies, Carlsbad, CA) and analyzed 24-48 hrs post-transfection.

RNA interference

All siRNA oligonucleotides were synthesized by Ambion^{R} Life Technologies (Applied Biosystems, Austin, TX). The following siRNAs were used for NM23-H1, SiH1: 5'-GGAUUCCGCCUUGUUGGUC; SiH1': 5'-GGAACACUACGUUGACCUG and siH1": 5'-GGCUGUAGGAAAUCUAGUU that targets the 3'-UTR region of NM23-H1; NM23-H2, SiH2: 5'-GGAUUGAUCAUUCUUUUAU and SiH2': 5'-GCCUAUGGUUUAAGCCUGA; NM23-H4, SiH4: 5'-GAUGCUGCAGGCACCAGAG; OPA1, SiOPA1: 5'-GAUCAUCUGCCACGGGUUG. Irrelevant control siRNA: 5'-GGCUGUAGAAGCUAUAGUU. HeLa cells were transfected with 50 nM control (mock) or specific siRNA duplex using Oligofectamine

reagent (Invitrogen Life Technologies, Carlsbad, CA). BSC-1 and Hep2 cells were transfected with Lullaby reagent (OZ Biosciences, Marseille, France). Protein depletion was verified by immunoblotting analysis with specific antibodies and was maximal after 72 hrs of siRNA treatment. Expression levels for experiments with NM23-H4 siRNA were determined with qPCR.

Flow cytometry-based endocytosis and recycling assays (EGF and Tf)

siRNA-treated cells were serum-starved for 30 min at 37°C in DMEM, then washed in PBS and detached with Versene solution (Invitrogen). Harvested cells were incubated for 1 h in ice-cold binding medium (DMEM supplemented with 1% BSA, 20 mM HEPES pH 7.4) containing 5 μg/mL Alexa488-conjugated human Tf or 100 ng/mL Alexa488-conjugated human EGF. After washing with ice-cold binding medium, cells were processed for endocytosis or recycling assay. For rescue experiment, cells treated with control or siH1" siRNAs were transfected either with pEGFP-N1 alone or pEGFP-N1 together with wild-type or NM23-H1^{H118N} mutant constructs. After serum-starvation and harvesting, cells were incubated with 100 ng/mL Alexa647-conjugated human EGF for 1 h and then assayed for endocytosis.

For endocytosis assay, cells were incubated in DMEM, 1% BSA, 20 mM HEPES at 37°C for the indicated times and quickly cooled on ice. After two washes in cold PBS, cells were acid-washed in ice-cold stripping medium (50 mM glycine, 100 mM NaCl, pH 3.0) for 2 min to remove surface-bound Tf or EGF. Cells were then washed in cold PBS and kept on ice in cold PBS before analysis.

For recycling assay, cells were incubated in DMEM, 1% BSA, 20 mM HEPES at 37°C for 6 min and cooled on ice. After two washing steps in cold PBS, cells were acid-washed in 50 mM glycine, 100 mM NaCl, pH 3.0 for 2 min on ice. Cells were then washed twice in cold PBS and incubated in DMEM, 1% BSA, 20 mM HEPES at 37°C for the indicated time to allow Tf recycling, and transferred on ice. Cells were then washed in cold PBS and kept on ice before analysis.

Cells were analyzed on a FACSCalibur system (BD Biosciences) measuring the fluorescence of Alexa488-Tf or -EGF or GFP and Alexa647-EGF. At least 10,000 cells were analyzed in each condition. Background fluorescence was measured from acid-washed cells after the binding step at 4°C and this value was subtracted from values at all time points.

Internalization of radiolabeled ^{125}I-EGF

Cells plated on 24-well plates and treated with the indicated siRNAs were serum-starved for 3 h. Cells were incubated in DMEM, 20mM HEPES, 0.1% bovine serum albumin with 1.5 ng/mL (low dose) or 100 ng/mL (high dose) ^{125}I-EGF at 37°C for the indicated time points. Cells were washed with ice-cold PBS and then acid-wash treated with 0.2 M acetic acid, pH 2.8, 0.5 M NaCl for 5 min on ice. The acid-wash solution was collected to determine the amount of surface-bound ^{125}I-EGF. Finally, cells were lysed in 1N NaOH to evaluate internalized ^{125}I-EGF. Nonspecific binding is measured for each time point in the presence of 300-fold molar excess of unlabeled EGF and is subtracted from the count. The rate of internalization is expressed as internalized/surface-bound radioactivity.

Immunofluorescence-based assay for endocytosis of IL-2Rβ

Endocytosis of the IL-2 receptor β subunit (IL-2Rβ) was measured at 37°C for 5 min as previously described (*22*). Briefly, Hep2 cells stably expressing IL-2Rβ were grown on coverslips and treated with the indicated siRNAs were incubated in DMEM, 0.5% BSA, pH 7.4 at 37°C for 5 min with 0.7 μg/coverslip of Cy3-conjugated anti-IL-2Rβ mouse antibody. Cells were fixed and permeabilized. Fluorescence images were obtained with an Apotome microscope (Zeiss) equipped with a x63 objective and a Roper Scientific Coolsnap HQ camera. A z-series of 1 μm optical sections was acquired. Images collected from three independent experiments (100 cells in each experiment) were further analyzed using the ICY software (http://icy.bioimageanalysis.org) using endosome number and fluorescence intensity as parameters.

Electron microscopy

For electron microscopy of CCPs, HeLa cells plated on coverslips were starved for 30 min and then incubated with Tf-Biotin conjugates for 1 h at 4°C. After washing, cells were incubated with anti-Biotin antibodies and protein-A gold conjugates (PAG 10). After the last washing steps, cells were incubated for 4 min at 37°C to allow internalization. Cells were fixed with 2.5% glutaraldehyde in 0.1 M cacodylate buffer (pH 7.4) and then processed for conventional electron microscopy as previously reported (*27*). Sections were observed under an electron microscope (Philips CM120; FEI Company, Eindoven, The Netherlands) and digital acquisitions were made with a numeric camera (Keen View; Soft Imaging System, Germany).

For electron microscopy of mitochondria, HeLa cells were seeded on Thermanox plastic coverslips (Nalge Nunc). Cells treated with NM23-H4 siRNA for 72 hrs were fixed for 30 min in 1% glutaraldehyde (Ted Pella Inc., Redding, CA), washed with PBS and incubated for 1 h with 1% osmium tetroxide. The samples were then dehydrated and embedded in Epon resin. 70-nm thick sections were stained with uranyl acetate and lead citrate. The sections were viewed with a JEOL electron microscope (JEOL Ltd., Tokyo, Japan).

Anti-NM23-immunogold-electron microscopy

BPL/5% PtdIns (4,5) P_2 were incubated with dynamin-1 and NM23-H2 in 20 mM HEPES, 100 mM NaCl, 1 mM $MgCl_2$, pH 7.4 in an Eppendorf centrifuge. The preparation was then fixed with 2% formaldehyde and pelleted. After washes in 20 mM HEPES, 100 mM NaCl, 1 mM $MgCl_2$, pH 7.4, the pellet was reacted sequentially with rabbit polyclonal pan-NM23 antibodies and protein A-gold conjugates. The sample was postfixed with 1% glutaraldehyde and treated with 0.4 M sodium phosphate buffer containing 2% osmium tetroxide for 1 h. The sample was stained with 0.25% uranyl acetate overnight and rinsed with ddH_2O followed by sequential dehydration in 30%, 50%, 70% and 90% ethanol for 5-10 min. The last dehydration step was carried out three times in absolute ethanol for 30 min each. The sample was then washed with propylene oxide twice for 10 min followed by incubation in epon-propylene oxide (1:1) for 1 h. Lastly, the sample was treated with 100% epon overnight at room temperature before being embedded in 1 mL of epon resin mix and curing at 65°C at least 24 h. Ultrathin sectioning was performed using a microtome (Leica Ultracut) at a cutting angle of 6°.

Sections were put on glow-discharged carbon-coated formvar grids and viewed with an electron microscope (Tecnai, 300 kV).

Immunofluorescence staining

Cells grown on glass coverslips were fixed with cold methanol and then incubated with the indicated primary antibodies. The secondary antibodies used were Alexa488-conjugated IgGs and Cy3-conjugated IgGs. Images were obtained by wide-field microscopy. For TIRF microscopy, cells grown on glass-coverslips, fixed and stained as above were imaged through a 100x 1.49 NA TIRF objective on a Nikon TE2000 (Nikon France SAS, Champigny sur Marne, France) inverted microscope equipped with a QuantEM EMCCD camera (Roper Scientific SAS, Evry, France/Photometrics, AZ, USA), a dual output laser launch which included 491 and 561 nm 50 mW DPSS lasers (Roper Scientific), and driven by Metamorph 7 software (MDS Analytical Technologies). A DV2 beam-splitter system (Roper Scientific/Photometrics) mounted on the light path enabled the simultaneous acquisition of the two emission channels. A motorized device driven by Metamorph allowed the accurate positioning of the illumination light for evanescent wave excitation.

Mitochondrial staining analysis and NM23-H4 immunodetection

For mitochondrial staining, HeLa cells were transfected with the indicated siRNAs and the mitochondrial marker mitoDsRED (Molecular Probes). Live cells were photographed with fluorescence microscopy and images for each siRNA were coded and pooled with images for the other siRNAs for unbiased classification. Cells were classified as having predominantly tubular or fragmented mitochondria as reported elsewhere (*28*).
For immunocytochemistry, HeLa cells grown on glass coverslips were fixed with 3.7% paraformaldehyde, permeabilized with 0.1% Triton X-100 in PBS, and incubated with polyclonal anti-NM23-H4 antibodies and monoclonal anti-OPA1 antibody. Secondary antibodies used were anti-rabbit IgG-FITC (Jackson ImmunoResearch) and anti-mouse IgG-Rhodamine (Biomeda). Fluorescence images were acquired with a 100X α Plan-Fluar/NA1.45 objective on a Zeiss Axiovert 200 M microscope, using a Hamamatsu ORCA ER camera controlled by Zeiss Axiovision software.

In situ proximity ligation assay (PLA)

To monitor the subcellular localization of protein-protein interactions at single molecule resolution, an *in situ* proximity ligation assay (PLA) was performed as previously described (*29*). Cells grown on coverslips were fixed with cold methanol and then incubated with primary antibodies. Secondary antibodies tagged with short DNA oligonucleotides were added. Hybridization, ligation, amplification and detection were realized according to the manufacturer's protocol (Olink Biosciences). Briefly, secondary antibodies were incubated in preheated humidity chamber for 1 h at 37°C. Ligation was performed with a ligase-containing ligation solution for 30 min at 37°C. Finally, amplification step was performed with a polymerase-containing amplification solution for 1h40 min at 37°C. After the PLA reaction, coverslips were further incubated with Alexa488-conjugated IgGs and Cy5-conjugated IgGs to detect proteins corresponding to the primary antibodies used. PLA signal corresponds to the Cy3 fluorescence. Coverslips were analyzed on an inverted wide-field microscope.

Measurement of NDPK activity

NDPK activity in cell lysates and of recombinant NM23 proteins was measured using a spectrophotometric pyruvate kinase/lactate deshydrogenase coupled assay as previously described (*23*). Briefly, the reaction mixture contained 50 mM HEPES, pH 7.4, 75 mM KCl, 5 mM $MgCl_2$, 1 mM phosphoenolpyruvate, 0.1 mM NADH, 1 mM ATP, 0.2 mM TDP, 1 mg/mL bovine serum albumin, and 2 U/mL each of pyruvate kinase and lactate deshydrogenase. NADH oxidation, which reflects the formation of adenosine diphosphate by NDPK, was followed spectrophotometrically by the decrease in absorbance at 334 nm during 2 min (measurement of absorbance every 12 s).

Subcellular fractionation

Cells were scrapped and resuspended in hypotonic buffer (10 mM HEPES, pH 7.5, 2.5 mM $MgCl_2$, 2 mM EGTA with a cocktail of protease inhibitors) by repeated passages through a 27G needle. The homogenate was centrifuged at 200*g* for 10 min at 4°C to yield a post-nuclear supernatant (PNS), which was centrifuged at 100,000*g* for 60 min at 4°C to yield supernatant and pellet fractions. Pellet was resuspended in hypotonic buffer to a volume equal the volume of supernatant, and equal volume of high-speed fractions and PNS were analyzed by immunoblotting using specific antibodies.

Immunoprecipitation

Cells or fresh mouse brain were lysed in 50 mM Tris-HCl pH 7.5, 137 mM NaCl, 10 mM MgCl2, 10% glycerol, 1% Triton-X100 with protease inhibitors and centrifuged at 16,000*g* for 10 min at 4°C. Supernatants were incubated with 2 μg of antibody for 2 h at 4°C and a 1:1 mixture of Protein-A and Protein-G Sepharose 4 Fast Flow (GE Healthcare) was added and further incubated for 1 h at 4°C. Beads were washed three times in lysis buffer, and bound proteins were eluted in SDS sample buffer and analyzed by immunoblotting with the indicated antibodies.

For analysis of direct binding *in vitro*, recombinant NM23-H2 (2 μg) and dynamin-2 (20 μg) were incubated in 50 mM Tris-HCl pH 7.5, 137 mM NaCl, 10 mM MgCl2, 10% glycerol, 1% Triton-X100 with protease inhibitors. NM23-H2 was immunoprecipitated as reported above with anti-NM23 IgGs and bound proteins were detected with anti-dynamin-2 antibodies.

Pull-down assay

For pull-down assay of NM23 proteins, HeLa cells were lysed in 50 mM Tris-HCl pH 7.5, 137 mM NaCl, 10 mM MgCl2, 10% glycerol, 1% Triton-X100 with protease inhibitors and centrifuged at 16,000*g* for 10 min at 4°C. Supernatants were incubated with the indicated GST fusion proteins for 1 h at 4°C in the presence of 0.5% BSA. Then, glutathione-Sepharose beads were added for 2 h at 4°C. Beads were washed and bound proteins were analyzed by SDS-PAGE and immunoblotting using specific anti-NM23-H1 or anti-NM23-H2 polyclonal antibodies.

Measurement of nucleoside diphosphate and triphosphate levels

Analysis of nucleoside diphosphates and triphosphates was performed by liquid chromatography coupled with tandem mass spectrometry as previously described (*30*).

Briefly, 100 mM standards of ATP, CTP, GTP, UTP and stable isotope labelled (^{13}C, ^{15}N) analogs were purchased in solution from Sigma-Aldrich (St Quentin-Fallavier, France). The calibration assay used stable isotope labelled analogs of each compound as standard and 8-bromoadenosine-5'-triphosphate was used as internal standard. As stable isotope labelled analogs of nucleoside diphosphates were not commercially available, their quantification was performed using the calibration curve of the nucleoside triphosphate analogs. Sample preparation from cells was performed with a protein precipitation step followed by a solid phase extraction (SPE) based on a weak-anion-exchange cartridge (*30*). The cartridges (Oasis® Wax - 60 mg; Waters, Milford, USA) were conditioned with 2 mL of methanol followed by 2 mL of ammonium acetate (50 mM, pH 4.5). This last step allowed improving nucleotides retention since at pH 4.5, WAX sorbent (pKa ~6) was under ionized form ($R4^{-}N^{+}$), which strongly improved ionic interactions with phosphate groups of nucleotides. Sample solutions were loaded onto the SPE cartridges, and after a slow percolation, the cartridges were washed with 2 mL ammonium acetate (50 mM, pH 4.5). Elution of the nucleotides from the cartridges was performed with 2 mL of a solution containing methanol/water/ammoniac (80/15/5; v/v/v). At basic pH, WAX sorbent was not ionized and the nucleotides were eluted. Eluate was evaporated to dryness under liquid nitrogen at 37°C and the residue was reconstituted in 100 µL solution methanol/water/ammoniac. Ten µL were then injected into the chromatographic device. The analytical separation of the nucleoside di- and triphosphates was achieved on a porous graphitic carbon stationary phase with a binary elution gradient program employing ion-pairing reagents and methanol. The triple quadrupole mass spectrometer operated in negative multiple reaction monitoring modes for all compounds and the fragmentation pathway corresponded to the loss of a pyrophosphate group. ATP and ADP were however detected in positive mode in order to distinguish them from dGTP and dGDP, which exhibit the same transition in negative mode. Intracellular concentrations of the nucleoside di- and triphosphates were expressed in pmol/10^6 cells (*31*).

GTPase assay

Liposome-stimulated GTPase activity of purified recombinant human dynamin-1, dynamin-2 and OPA1 was evaluated by monitoring released inorganic phosphate, which was quantitated by a colorimetric method (*32*). The color reagent was prepared by combining 30 mL malachite-green solution (0.045% m/v) with 20 mL ammonium molybdate in 4 M hydrochloric acid (4.2% m/v) followed by filtration through 0.2-µm filter. To measure specifically the dynamin-1/-2 GTPase activity, the reaction was performed in a volume of 50 µL with 2 µg lipids (95% BPL/5% PIP_2), 1 µg dynamin-1 or -2, nucleotides at the different concentrations indicated for each experiment and NM23-H1/-H2 purified recombinant proteins in 20 mM HEPES, 100 mM NaCl, 1 mM $MgCl_2$, pH 7.4. For measurement of OPA1 GTPase activity, the reaction was performed in a volume of 50 µL with 10 µg lipids (45% POPC/22% POPE/8% PIP_2/25% cardiolipin), 10 µg purified recombinant OPA1, nucleotides at the different concentrations indicated for each experiment and NM23-H4 purified recombinant protein in 20 mM HEPES, 100 mM NaCl, 1 mM $MgCl_2$, pH 7.4. The reaction mixture was incubated for increasing time at 37°C. After addition of the malachite-green reagent, the absorbance was measured with a spectrophotometer at 650 nm against a standard solution of Pi.

In vitro fission assay

The effect of NM23 on dynamin-mediated fission of membrane tubules was analyzed using a light-microscopy-based assay as previously reported (*6*). Briefly, lipids (95% BPL/5% PIP2) were spotted in a small chamber between two glass surfaces and dried. Lipids were fully rehydrated by filling the chamber by capillary action with 15-20 μL of GTPase buffer (20 mM HEPES, 100 mM NaCl, 1 mM $MgCl_2$, pH 7.4) containing 0.5 mg/mL casein to block the glass surface and to avoid sticking of proteins on the surface. Rehydration generated membrane sheets. The dynamin-containing solution (2 mg/mL) was then applied to the chamber and the deformation of membrane sheets produced by its diffusion into the chamber was recorded by differential interference contrast (DIC) microscopy. The NM23-containing solution (2 mg/mL) was added after formation of the tubes. A washing step with GTPase buffer was performed just before the addition of nucleotides (1 mM ATP and 1 mM GDP) in the same buffer to discard excess soluble NM23-H1/H2. Experiments were performed with rat brain dynamin and human dynamin-1. All incubations were carried out at room temperature.

Electron microscopy analysis of negatively stained tubules

Negative staining electron microscopy of dynamin-coated lipid tubules in the absence and presence of NM23 was performed according to (*33*). Briefly, lipids (95% BPL/5% PIP_2) were incubated with either human dynamin-1 alone or with human dynamin-1 and NM23-H2 proteins in 20 mM HEPES, 100 mM NaCl, 1 mM $MgCl_2$, pH 7.4 during 5 min and applied on a carbon-grid for 3 min. Then, a washing step in 20 mM HEPES, 100 mM NaCl, 1 mM $MgCl_2$, pH 7.4 was performed before adding dye.

Statistical analyses

Statistical analyses were performed using an unpaired Student's *t*-test in Microsoft excel software. All Student's *t*-tests were two-sided. The level of statistical significance was set at <0.05.

Supplementary Acknowledgments

M.B. was the recipient of a postdoctoral fellowship from the Ligue Nationale contre le Cancer. T.L. was supported by a grant from Institut Pasteur (PTR 387). Core funding for this work was provided by Institut Curie and Centre National pour la Recherche Scientifique and additional support was provided by grants from the Fondation ARC pour la Recherche sur le Cancer (SL220100601356) to PC. This work was supported by grants of the Groupement des Entreprises Françaises contre le Cancer (GEFLUC; to M.L.L and M.B.) and the Fondation pour la Recherche Médicale (FRM; DPM20121125557 to U.S and M.B.) and grants from the Human Frontier Science Program CDA-0061-08, the Swiss National Fund for Research Grant N°31003A_130520 and the European Research Council Starting Grant N°311536 (2011 call) to A.R.

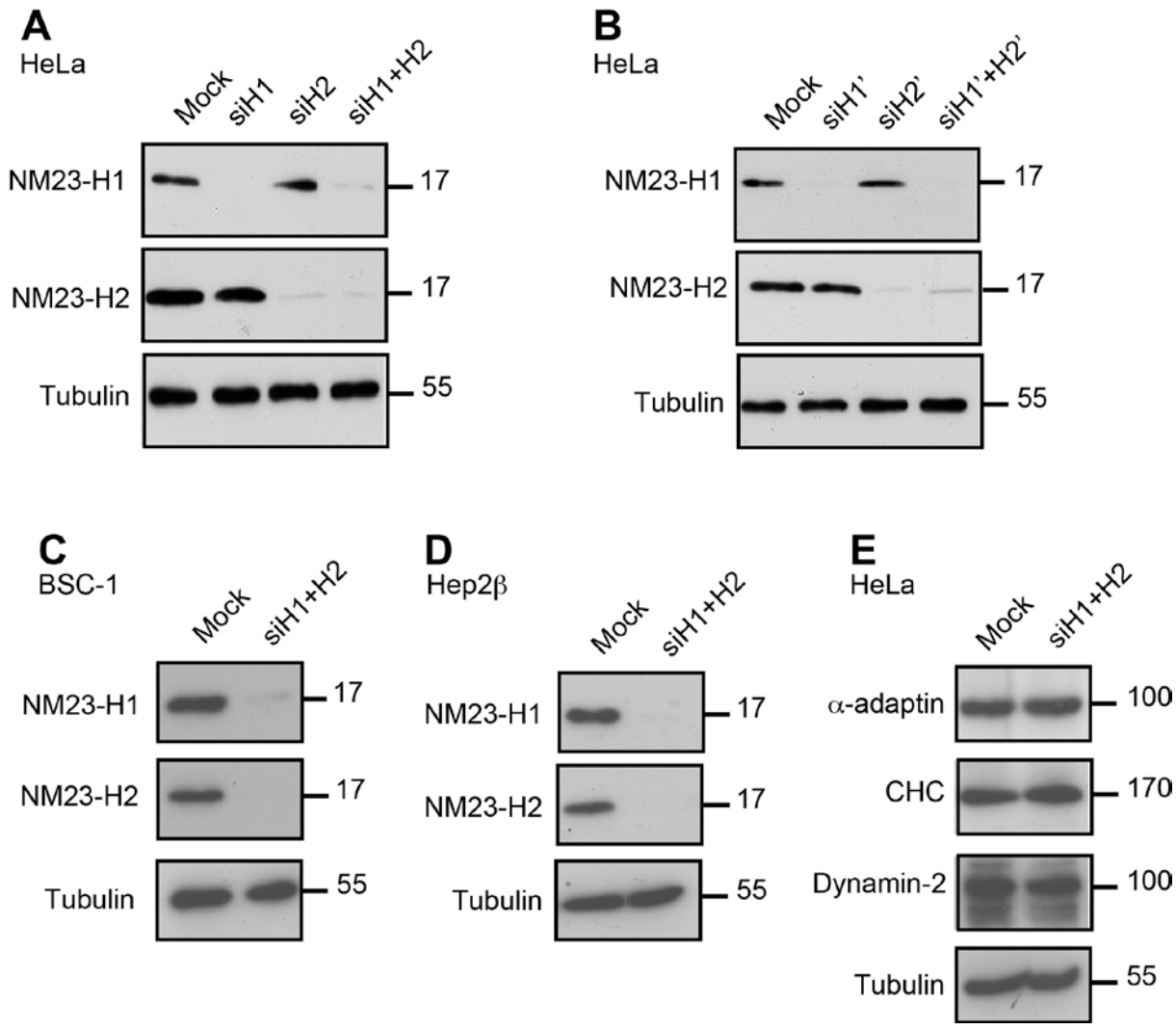

Fig. S1.

Suppression of NM23-H1 and NM23-H2 expression with specific siRNAs does not affect levels of key endocytic components in mammalian cells.

(A) and **(B)** Specific expression of NM23-H1 and NM23-H2 was analyzed by immunoblotting with polyclonal specific affinity-purified anti-NM23-H1 and anti-NM23-H2 antibodies in HeLa cells mock-treated or transfected with different single siRNAs against NM23-H1 (siH1, siH1'), NM23-H2 (siH2, siH2'), and with the combination siH1+H2 or siH1'+H2'. **(C)** Specific expression of NM23-H1 and NM23-H2 was analyzed by immunoblotting in BSC-1 cells mock-treated or transfected with siH1+H2. **(D)** Specific expression of NM23-H1 and NM23-H2 was analyzed by immunoblotting in Hep2β cells (Hep2 cells stably transfected with IL-2 receptor β subunit) mock-treated or transfected with siH1+H2. **(E)** Expression of three major endocytic proteins, α-adaptin, clathrin heavy chain (CHC), and dynamin-2 was analyzed by immunoblotting in HeLa cells and was unaffected upon NM23-H1/-H2 silencing. Control for equal loading was obtained by immunoblotting with anti-tubulin antibody. Molecular weights are indicated in kDa.

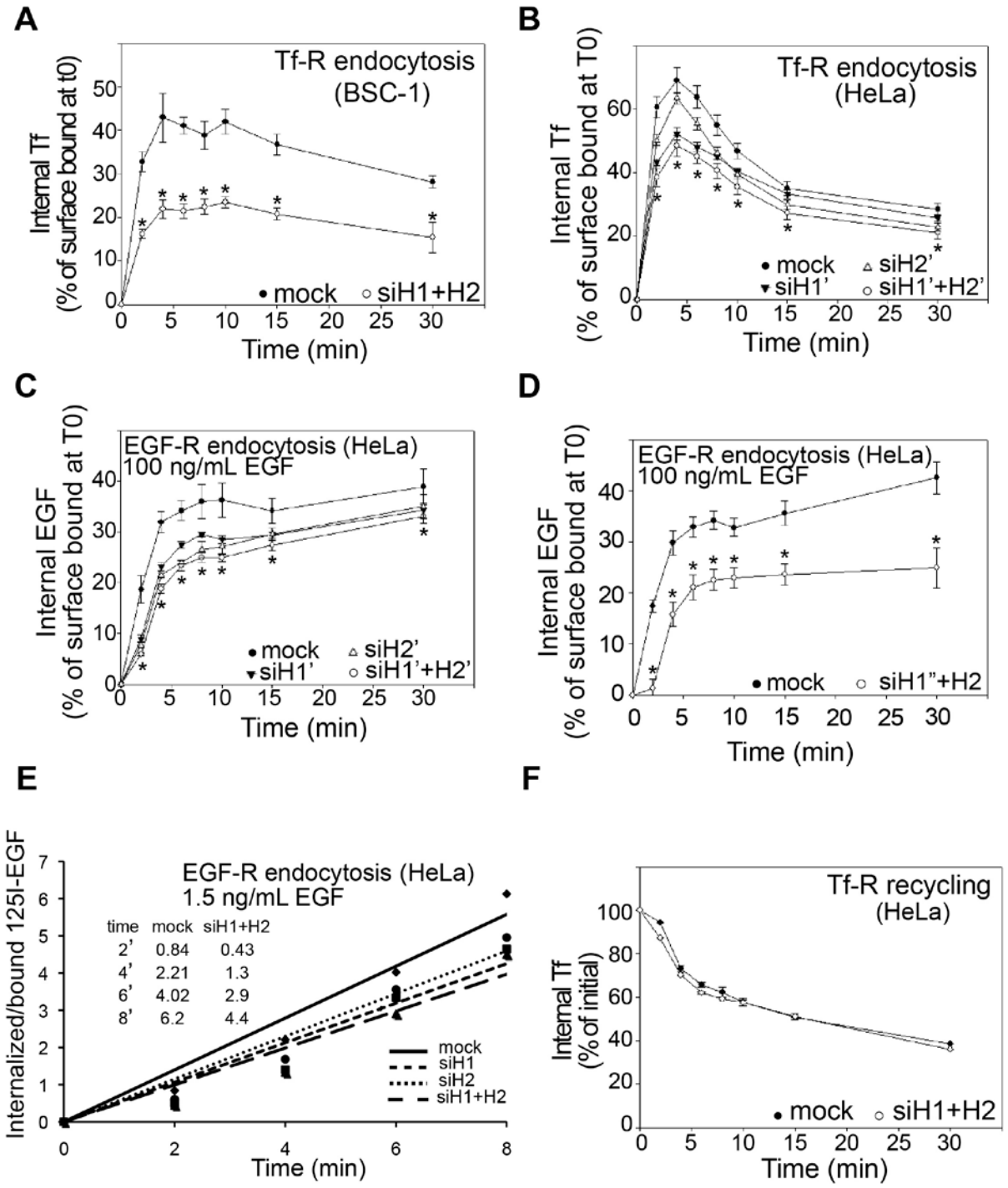

Fig. S2

NM23-H1/H2 knockdown with different sets of siRNA impairs dynamin-dependent endocytosis without affecting recycling.

(A) BSC-1 cells were mock-treated or treated with a pair of siRNAs to simultaneously knockdown NM23-H1 and NM23-H2 and assessed for endocytosis of Alexa488-Tf. Data are expressed as percentage of internal Tf compared to surface-bound Tf at time 0 ± SEM from four independent experiments. *, $P < 0.05$ compared to mock-treated cells. **(B)**

HeLa cells were mock-treated (black circle), or transfected with siH1' (black triangle), siH2' (white triangle), siH1'+H2' (white circle) and assessed for endocytosis of Alexa488-Tf. Data are expressed as percentage of internal Tf compared to surface-bound Tf at time 0 ± SEM from four independent experiments. *, $P < 0.05$ when compared siH1'+H2' to mock-treated cells. **(C-D)** HeLa cells were assessed for endocytosis of EGR-receptor in response to high dose (100 ng/ml) of Alexa488-EGF under the various indicated conditions. Data are expressed as percentage of internal EGF compared to surface-bound EGF at time 0 ± SEM from four independent experiments. *, $P < 0.05$ when compared to mock-treated cells. **(E)** Kinetics of internalization of radio-labelled EGF (1.5 ng/mL) in HeLa cells under the various indicated conditions. Results are the average of triplicate points (SEM < 10%) and representative of three independent experiments. The interpolation curves are shown. The real values of the ratio internalized/surface-bound radio-labelled EGF for the control and siH1+H2 conditions are indicated. **(F)** HeLa cells were mock-treated (black circle) or transfected with siH1+H2 (white circle) and assessed for recycling of Alexa488-Tf. Data are expressed as percentage of internal Tf compared to time 0 ± SEM from four independent experiments. Of note, silencing of NM23-H1/H2 did not significantly affect the recycling of Tf-R.

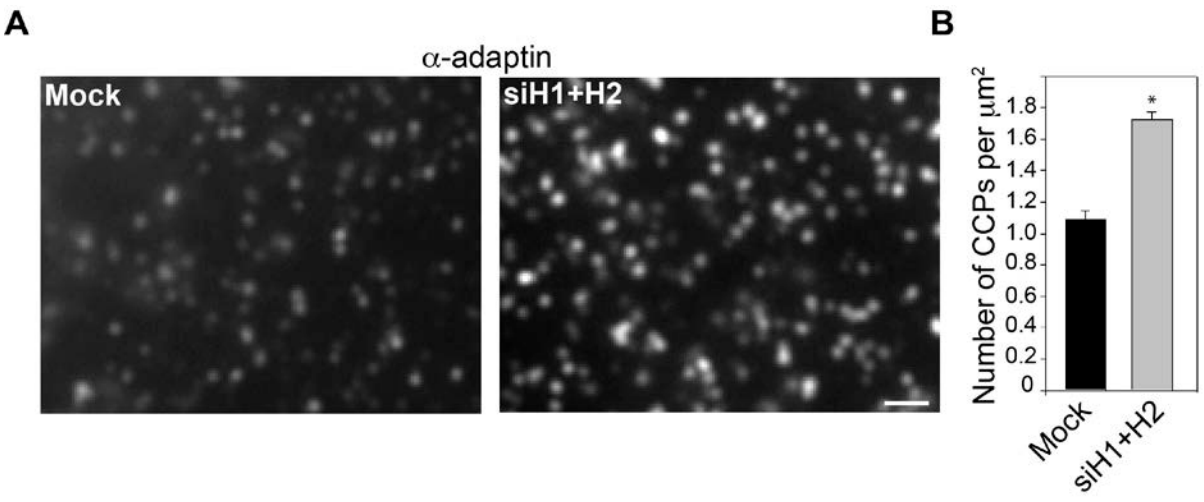

Fig. S3

Increased CCP density in BSC-1 cells depleted for NM23-H1/H2.

(A) AP-2 staining (α-adaptin) in BSC-1 cells knocked-down for NM23-H1/H2. Scale bar, 1 μm. **(B)** Mean CCP number/μm^2 ± SEM (n=10 cells for each condition). *, $P < 0.05$ compared to mock-treated cells.

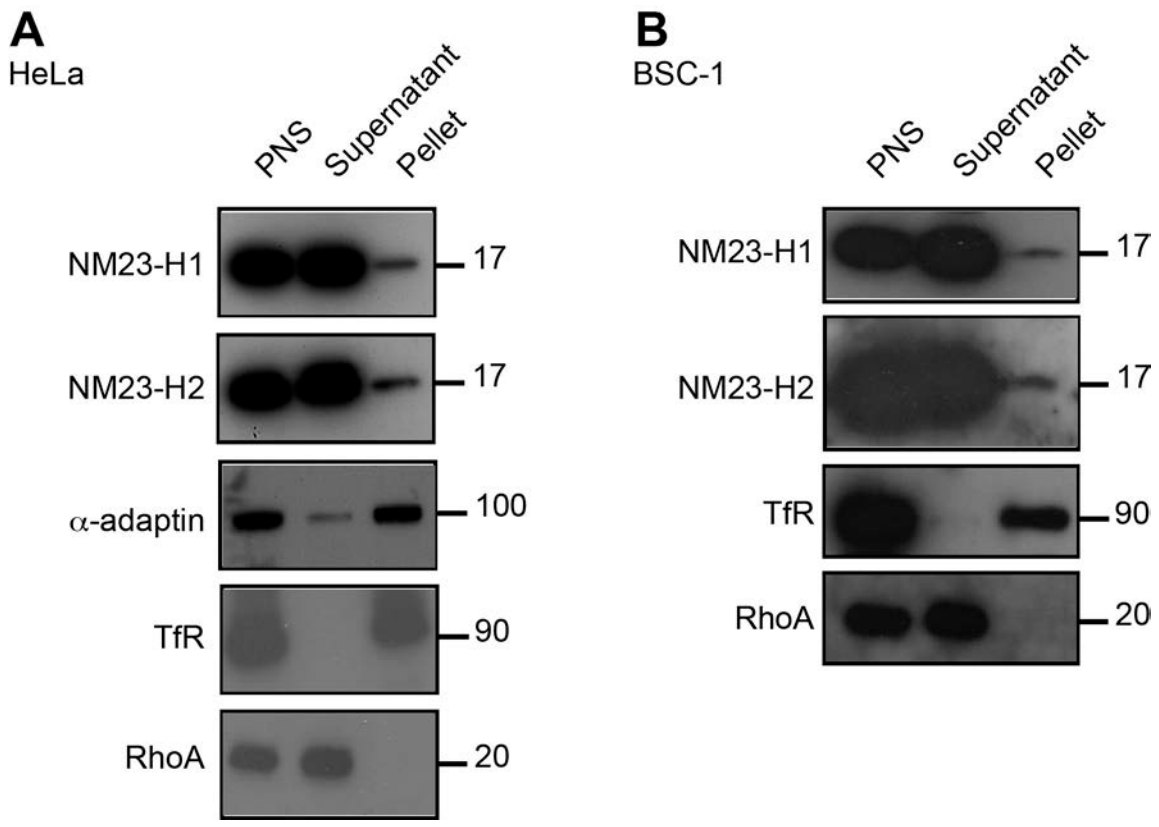

Fig. S4

NM23-H1 and NM23-H2 are membrane-associated.

(A, B) HeLa (A) and BSC-1 (B) cells were homogenized and a postnuclear supernatant (PNS) was prepared and centrifuged at 100,000*g* to produce a soluble (supernatant) and a membrane (pellet) fraction. Proteins corresponding to equivalent cell-number were loaded in each lane. The presence of NM23-H1, NM23-H2, α-adaptin, transferrin receptor (TfR, integral membrane protein) as well as RhoA (soluble protein) were detected in the fractions by immunoblotting analysis with specific antibodies. Two independent subcellular fractionations were performed and gave similar results. At long exposition, no signal of RhoA is detected in the pellet fraction (data not shown)

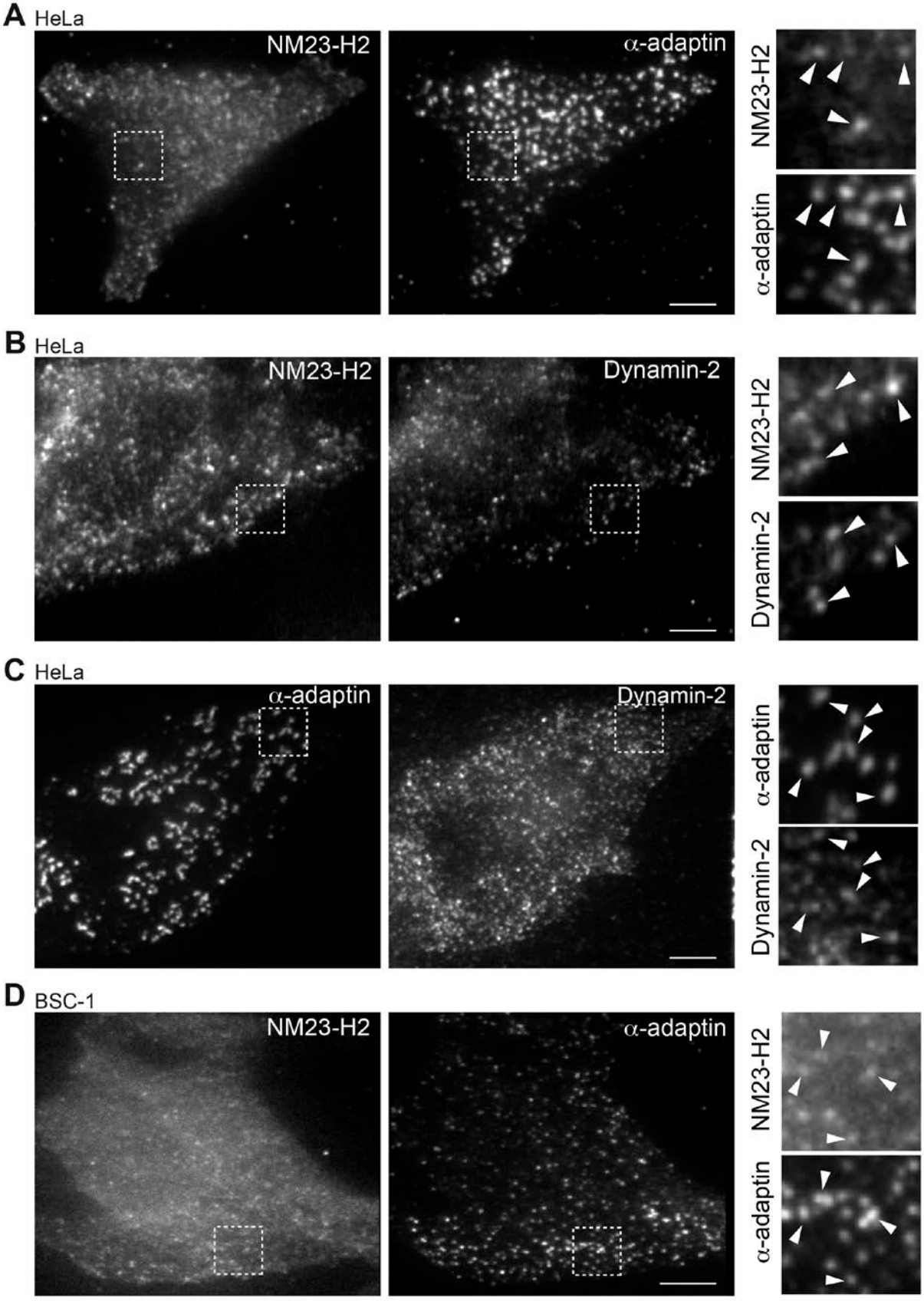
A HeLa
NM23-H2
α-adaptin
NM23-H2
α-adaptin
B HeLa
NM23-H2
Dynamin-2
NM23-H2
Dynamin-2
C HeLa
α-adaptin
Dynamin-2
α-adaptin
Dynamin-2
D BSC-1
NM23-H2
α-adaptin
NM23-H2
α-adaptin

Fig. S5

NM23 colocalizes with AP-2 and dynamin-2 in HeLa and BSC-1 cells.
(A, B) Immunofluorescence (TIRF microscopy) staining for endogenous NM23-H2 and α-adaptin AP-2 subunit (A) or dynamin-2 (B) in HeLa cells. Insets show co-localization of NM23-H2 with α-adaptin- and dynamin-2-labeled CCPs (arrowheads). Scale bar, 5 μm. **(C)** Immunolabeling (TIRF microscopy) for endogenous dynamin-2 and α-adaptin in HeLa cells. Insets show dynamin-2 colocalizing with α-adaptin. Scale bar, 5 μm. **(D)** Immunolabeling (TIRF microscopy) for endogenous NM23-H2 and α-adaptin in BSC-1 cells. Insets show NM23-H2 colocalizing with α-adaptin. Scale bar, 5 μm.

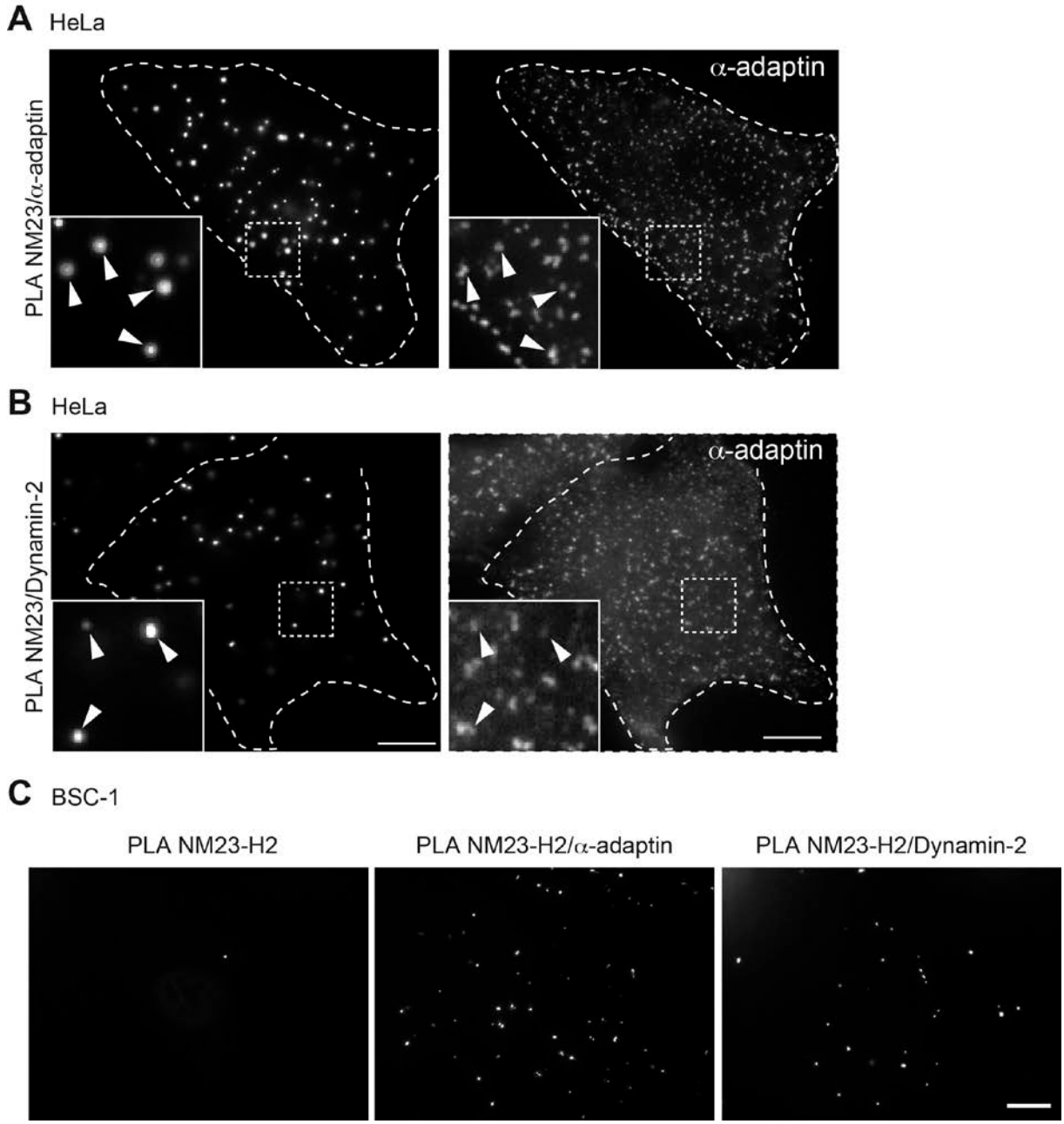

Fig. S6

NM23 associates with dynamin-2 in AP-2-positive CCPs.

(A, B) PLA signal using NM23 antibody in combination with α-adaptin antibody (A), or dynamin-2 antibody (B) in HeLa cells. Immunolabeling of α-adaptin was performed after PLA (right panels). Insets show PLA signals (NM23/α-adaptin or NM23/dynamin-2) colocalizing with α-adaptin-positive CCPs (arrowheads). PLA signal indicates a close proximity, possibly *in situ* interaction of NM23 with AP-2 and dynamin-2 at CCPs. Scale bar, 5 μm. **(C)** PLA signal using NM23-H2 antibody alone (left panel) or in combination with α-adaptin antibody (middle panel), or dynamin-2 antibody (right panel) in BSC-1

cells. One cell is shown in each panel. High PLA signal is observed in the presence of combined primary antibodies. Scale bar, 5 μm.

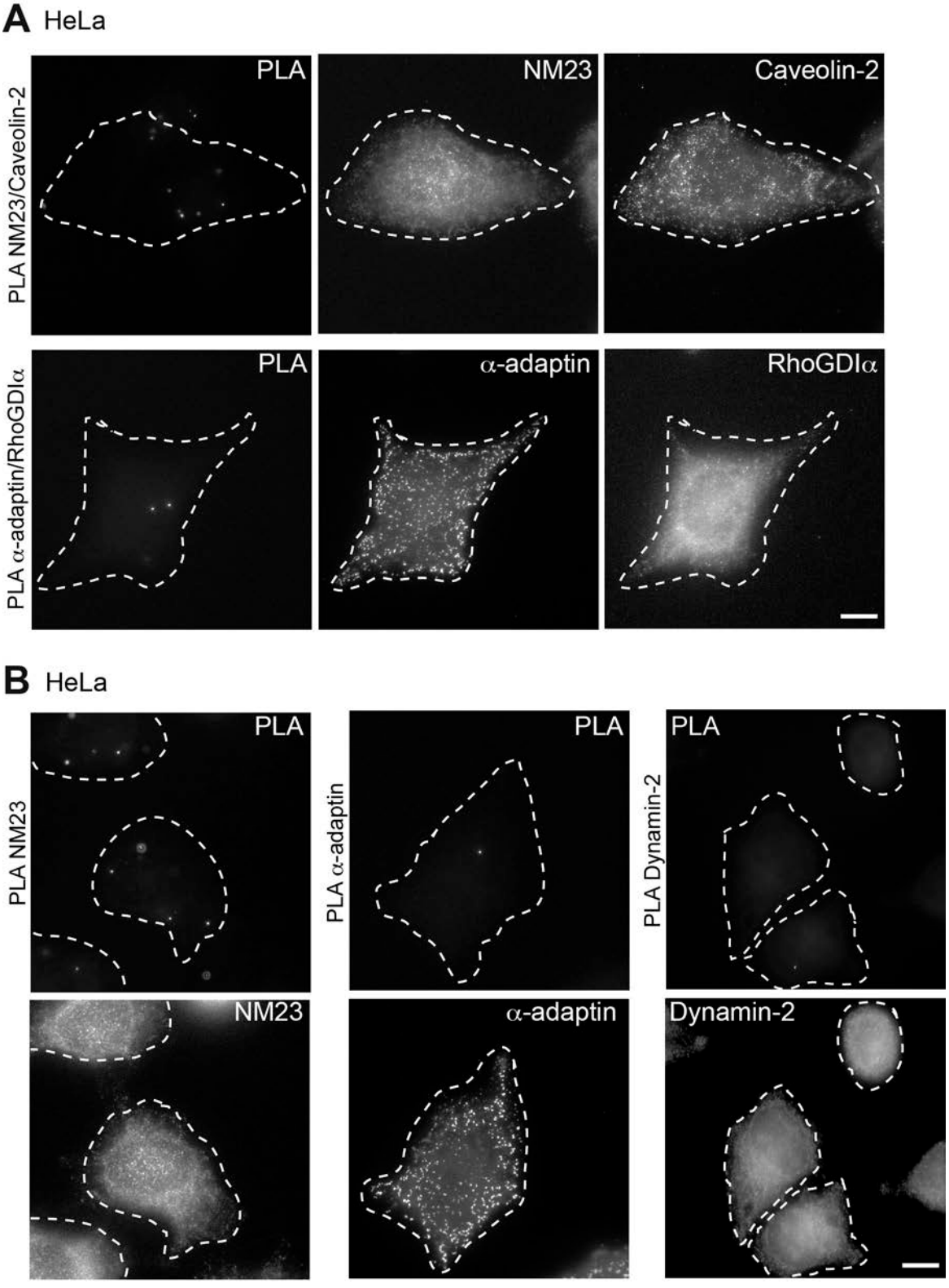

Fig. S7

NM23 is not associated with caveolae.

(A) PLA signal in HeLa cells between NM23 and caveolin-2, a component of caveolae (upper panel), and between α-adaptin and the cytosolic protein RhoGDIα (lower panel). Immunolabeling for each protein was performed after the PLA reaction. Dotted delimited single cells. Background PLA signal is observed when probing an association between NM23 and caveolin-2 indicating that NM23 is not associated with caveolae. Background signal is also observed between α-adaptin and RhoGDIα documenting the specificity of α-adaptin and NM23 association. Scale bar, 5 μm. **(B)** PLA signal in HeLa cells in the presence of only one primary antibody either directed against NM23 or α-adaptin or dynamin-2 (upper panel). Immunolabeling for each protein was performed after the PLA reaction (lower panel). Dotted delimited individual cells. Background signal is observed whatever the tested primary antibody. Scale bar, 5 μm.

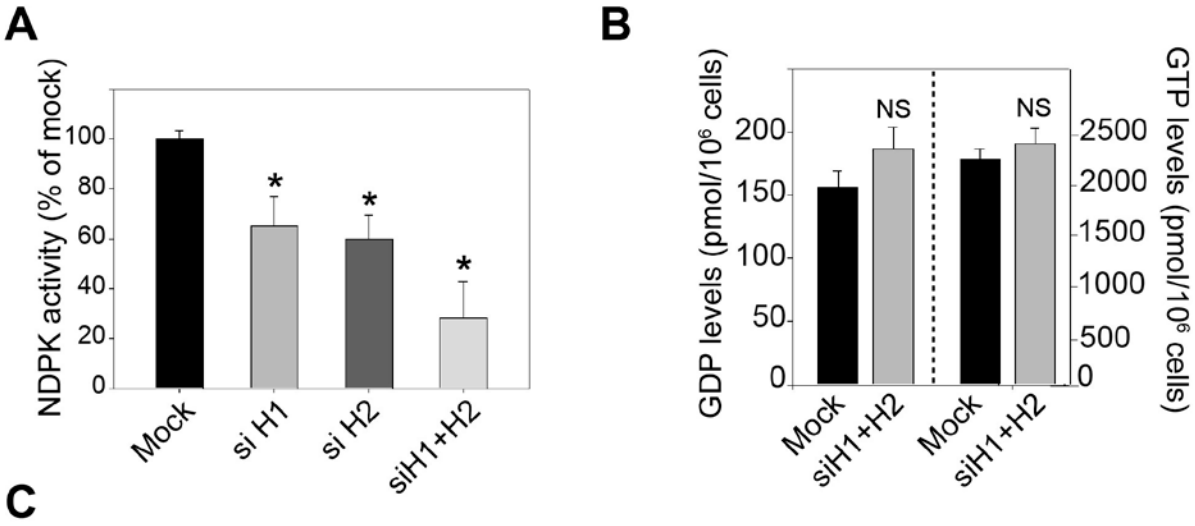

C

Triphosphate nucleosides	mock (pmol/10^6 cells)	siH1+H2 (pmol/10^6 cells)
ATP	7483±488	7211±595
GTP	2150±98	2298±149
UTP	2665±19	2854±294
CTP	1046±15	1147±68
Diphosphate nucleosides	mock (pmol/10^6 cells)	siH1+H2 (pmol/10^6 cells)
ADP	3761±187	4051±477
GDP	156±13	187±17
UDP	213±30	213±30
CDP	62±8	65±5
Ratio	mock	siH1+H2
ATP/ADP	2	1,8
GTP/GDP	13,8	12,3
UTP/UDP	12,5	13,4
CTP/CDP	16,9	17,6

Fig. S8

Overall intracellular GTP levels are unchanged upon NM23 inactivation.

(A) NDPK activity in HeLa cells mock-treated or transfected with siH1, siH2, and siH1+H2. Data are mean ± SEM of three independent experiments, each performed in duplicate. *, $P < 0.05$ compared to mock-treated cells. **(B)** Intracellular GDP and GTP levels in mock- and siH1+H2-treated HeLa cells measured by liquid chromatography coupled with tandem mass spectrometry. Data are mean ± SEM of three independent experiments. NS, not statistically significative compared to mock-treated cells. **(C)** Intracellular levels of the different nucleoside diphosphates and triphosphates in mock- and siH1+H2-treated HeLa cells measured as in B. Data are mean ± SEM of three

independent experiments. The results are expressed in pmol/10^6 cells. The ratio of nucleoside triphosphates/nucleoside diphosphates is shown.

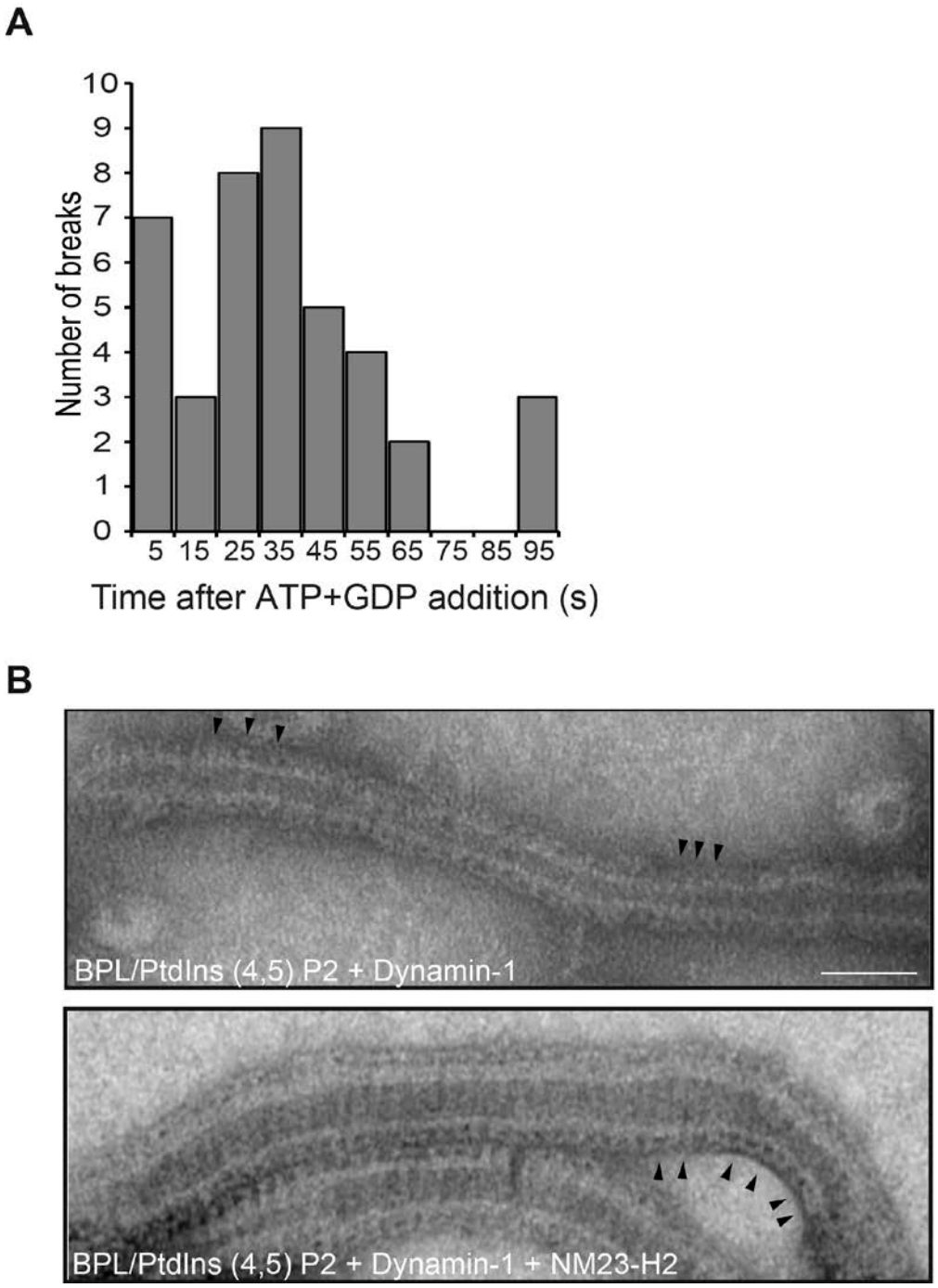

Fig. S9

NM23 associates with dynamin-coated tubules and promotes fission.

(A) Number of breaks of rat brain dynamin-coated tubules in the presence of NM23-H2 plotted as a function of time after addition of 1 mM ATP and 1 mM GDP. **(B)** Negative staining electron microscopy of liposomes incubated with dynamin-1 alone (upper panel). Arrowheads point to typical striations of the dynamin helical polymer around the tubules. In the lower panel, dynamin-1 was added together with NM23-H2. Arrowheads point to

thicker stripes than the dynamin-only coat very likely corresponding to the association of NM23-H2 to the surface of dynamin-1-coated tubules. Scale bar, 100 nm.

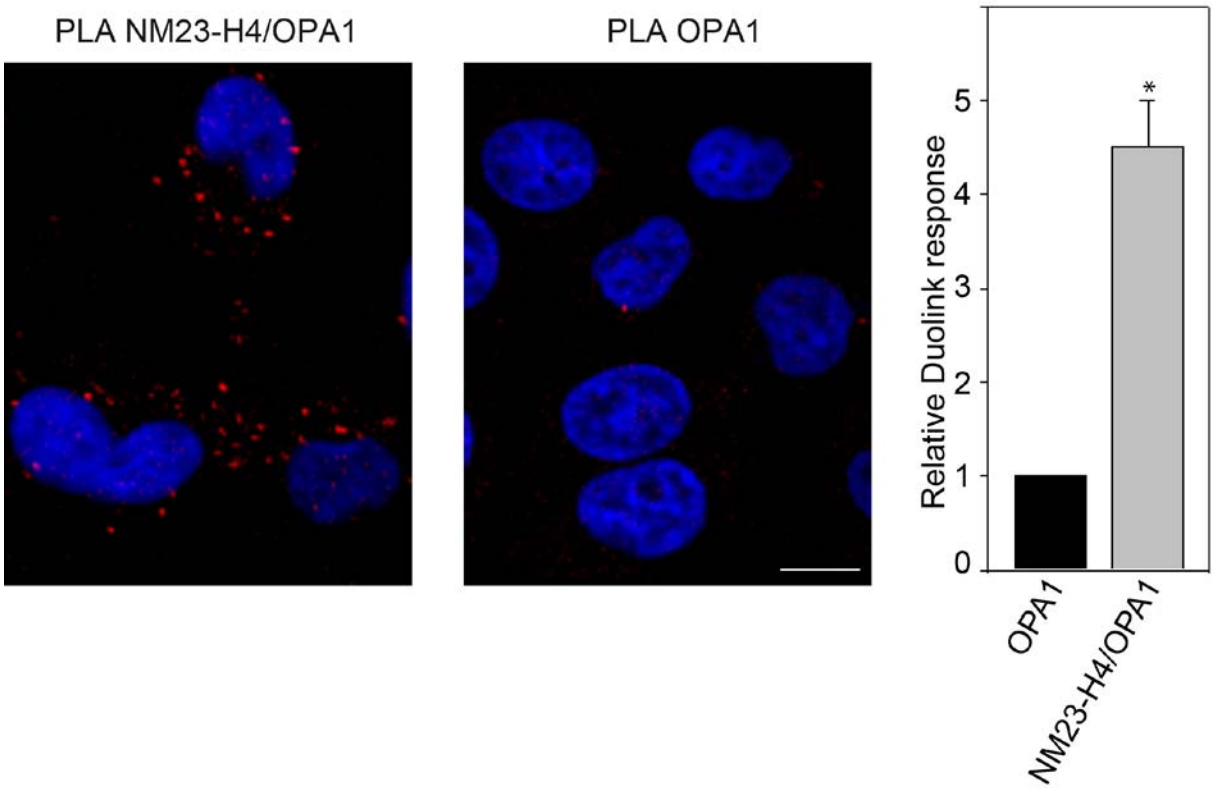

Fig. S10

Proximity ligation assay of NM23-H4 and OPA1.

PLA signal in HeLa cells between NM23-H4 and OPA1 (left panel) and in control reaction using only primary antibody against OPA1 (middle panel). Scale bar, 10 μm. Quantification is shown in the right panel from three independent experiments. *, $P <$ 0.01 compared to control OPA1-only PLA signal.

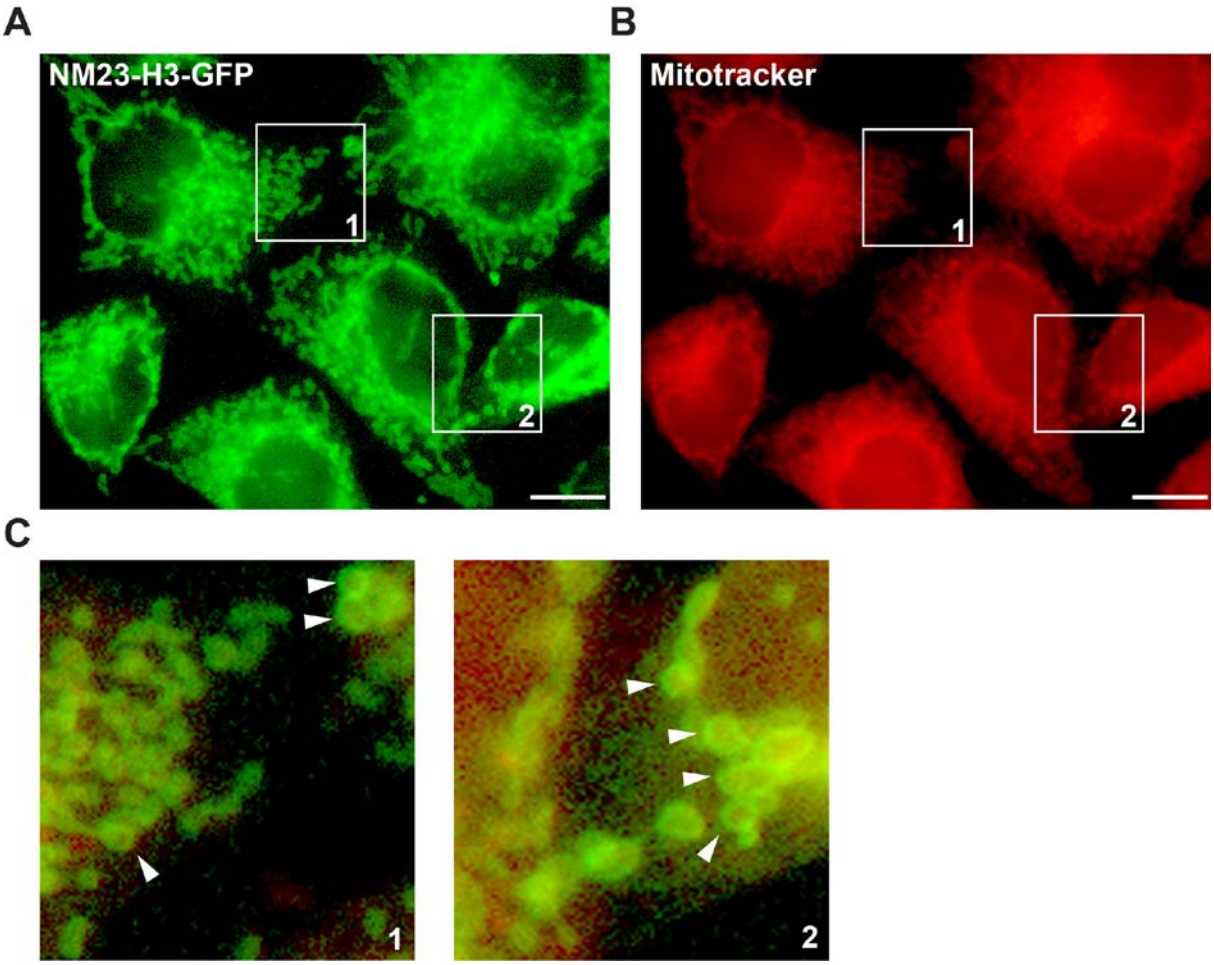

Fig. S11

NM23-H3 is associated with the mitochondrial outer membrane.

HeLa cells stably expressing full-length NM23-H3 protein C-terminally fused to GFP were incubated with mitochondrion-selective dye MitoTracker™ Red CMXRos for 30 min at 37°C and fixed. Staining of NM23-H3-GFP (A) and MitoTracker (B) are shown. Panel C show higher magnification of boxed regions indicating that NM23-H3-GFP is localized at the mitochondrial outer membrane (arrowheads point to a ring of NM23-H3-GFP at the periphery of mitochondria). Scale bar, 10 μm.

Movie S1

Effect of 1 mM ATP and 1 mM GDP, in the absence of NM23, on a network of dynamin-coated lipid tubules.
Dynamin was added before starting the time-lapse sequence. Images were taken every sec. Note the change in focus corresponding to nucleotide addition. Same field as in Fig. 3G.

Movie S2

Effect of 1 mM ATP and 1 mM GDP in the presence of NM23-H1 on a network of dynamin-coated lipid tubules.
Dynamin and NM23-H1 were added before starting the time-lapse sequence. Images were taken every sec. Note the change in focus corresponding to nucleotide addition. Same field as in Fig. 3G.

Movie S3

Effect of 1 mM ATP and 1 mM GDP in the presence of NM23-H2 on a network of dynamin-coated lipid tubules.
Dynamin and NM23-H2 were added before starting the time-lapse sequence. Images were taken every sec. Note the change in focus corresponding to nucleotide addition. Same field as in Fig. 3G.

References and Notes

1. S. M. Ferguson, P. De Camilli, Dynamin, a membrane-remodelling GTPase. *Nat. Rev. Mol. Cell Biol.* **13**, 75–88 (2012). Medline

2. S. L. Schmid, V. A. Frolov, Dynamin: Functional design of a membrane fission catalyst. *Annu. Rev. Cell Dev. Biol.* **27**, 79–105 (2011). Medline doi:10.1146/annurev-cellbio-100109-104016

3. J. E. Hinshaw, S. L. Schmid, Dynamin self-assembles into rings suggesting a mechanism for coated vesicle budding. *Nature* **374**, 190–192 (1995). Medline doi:10.1038/374190a0

4. K. Takei, P. S. McPherson, S. L. Schmid, P. De Camilli, Tubular membrane invaginations coated by dynamin rings are induced by GTP-γ S in nerve terminals. *Nature* **374**, 186–190 (1995). Medline doi:10.1038/374186a0

5. S. M. Sweitzer, J. E. Hinshaw, Dynamin undergoes a GTP-dependent conformational change causing vesiculation. *Cell* **93**, 1021–1029 (1998). Medline doi:10.1016/S0092-8674(00)81207-6

6. A. Roux, K. Uyhazi, A. Frost, P. De Camilli, GTP-dependent twisting of dynamin implicates constriction and tension in membrane fission. *Nature* **441**, 528–531 (2006). Medline doi:10.1038/nature04718

7. S. Morlot, V. Galli, M. Klein, N. Chiaruttini, J. Manzi, F. Humbert, L. Dinis, M. Lenz, G. Cappello, A. Roux, Membrane shape at the edge of the dynamin helix sets location and duration of the fission reaction. *Cell* **151**, 619–629 (2012). Medline doi:10.1016/j.cell.2012.09.017

8. D. D. Binns, M. K. Helms, B. Barylko, C. T. Davis, D. M. Jameson, J. P. Albanesi, J. F. Eccleston, The mechanism of GTP hydrolysis by dynamin II: A transient kinetic study. *Biochemistry* **39**, 7188–7196 (2000). Medline doi:10.1021/bi000033r

9. B. Marks, M. H. Stowell, Y. Vallis, I. G. Mills, A. Gibson, C. R. Hopkins, H. T. McMahon, GTPase activity of dynamin and resulting conformation change are essential for endocytosis. *Nature* **410**, 231–235 (2001). Medline doi:10.1038/35065645

10. K. S. Krishnan, R. Rikhy, S. Rao, M. Shivalkar, M. Mosko, R. Narayanan, P. Etter, P. S. Estes, M. Ramaswami, Nucleoside diphosphate kinase, a source of GTP, is required for dynamin-dependent synaptic vesicle recycling. *Neuron* **30**, 197–210 (2001). Medline doi:10.1016/S0896-6273(01)00273-2

11. V. Dammai, B. Adryan, K. R. Lavenburg, T. Hsu, *Drosophila* awd, the homolog of human nm23, regulates FGF receptor levels and functions synergistically with shi/dynamin during tracheal development. *Genes Dev.* **17**, 2812–2824 (2003). Medline doi:10.1101/gad.1096903

12. G. Nallamothu, J. A. Woolworth, V. Dammai, T. Hsu, Awd, the homolog of metastasis suppressor gene Nm23, regulates *Drosophila* epithelial cell invasion. *Mol. Cell. Biol.* **28**, 1964–1973 (2008). Medline doi:10.1128/MCB.01743-07

13. M. Boissan, S. Dabernat, E. Peuchant, U. Schlattner, I. Lascu, M. L. Lacombe, The mammalian Nm23/NDPK family: From metastasis control to cilia movement. *Mol. Cell. Biochem.* **329**, 51–62 (2009). Medline doi:10.1007/s11010-009-0120-7

14. L. Milon, P. Meyer, M. Chiadmi, A. Munier, M. Johansson, A. Karlsson, I. Lascu, J. Capeau, J. Janin, M. L. Lacombe, The human nm23-H4 gene product is a mitochondrial nucleoside diphosphate kinase. *J. Biol. Chem.* **275**, 14264–14272 (2000). Medline doi:10.1074/jbc.275.19.14264

15. M. Tokarska-Schlattner, M. Boissan, A. Munier, C. Borot, C. Mailleau, O. Speer, U. Schlattner, M. L. Lacombe, The nucleoside diphosphate kinase D (NM23-H4) binds the inner mitochondrial membrane with high affinity to cardiolipin and couples nucleotide transfer with respiration. *J. Biol. Chem.* **283**, 26198–26207 (2008). Medline doi:10.1074/jbc.M803132200

16. A. M. van der Bliek, Q. Shen, S. Kawajiri, Mechanisms of mitochondrial fission and fusion. *Cold Spring Harb. Perspect. Biol.* **5**, a011072 (2013). Medline doi:10.1101/cshperspect.a011072

17. S. M. Ferguson, A. Raimondi, S. Paradise, H. Shen, K. Mesaki, A. Ferguson, O. Destaing, G. Ko, J. Takasaki, O. Cremona, E. O' Toole, P. De Camilli, Coordinated actions of actin and BAR proteins upstream of dynamin at endocytic clathrin-coated pits. *Dev. Cell* **17**, 811–822 (2009). Medline doi:10.1016/j.devcel.2009.11.005

18. G. J. Praefcke, H. T. McMahon, The dynamin superfamily: Universal membrane tubulation and fission molecules? *Nat. Rev. Mol. Cell Biol.* **5**, 133–147 (2004). Medline doi:10.1038/nrm1313

19. L. Griparic, N. N. van der Wel, I. J. Orozco, P. J. Peters, A. M. van der Bliek, Loss of the intermembrane space protein Mgm1/OPA1 induces swelling and localized constrictions along the lengths of mitochondria. *J. Biol. Chem.* **279**, 18792–18798 (2004). Medline doi:10.1074/jbc.M400920200

20. U. Schlattner, M. Tokarska-Schlattner, S. Ramirez, Y. Y. Tyurina, A. A. Amoscato, D. Mohammadyani, Z. Huang, J. Jiang, N. Yanamala, A. Seffouh, M. Boissan, R. F. Epand, R. M. Epand, J. Klein-Seetharaman, M. L. Lacombe, V. E. Kagan, Dual function of mitochondrial Nm23-H4 protein in phosphotransfer and intermembrane lipid transfer: A cardiolipin-dependent switch. *J. Biol. Chem.* **288**, 111–121 (2013). Medline doi:10.1074/jbc.M112.408633

21. I. Lascu, S. Schaertl, C. Wang, C. Sarger, A. Giartosio, G. Briand, M. L. Lacombe, M. Konrad, A point mutation of human nucleoside diphosphate kinase A found in aggressive neuroblastoma affects protein folding. *J. Biol. Chem.* **272**, 15599–15602 (1997). Medline doi:10.1074/jbc.272.25.15599

22. A. Grassart, A. Dujeancourt, P. B. Lazarow, A. Dautry-Varsat, N. Sauvonnet, Clathrin-independent endocytosis used by the IL-2 receptor is regulated by Rac1, Pak1 and Pak2. *EMBO Rep.* **9**, 356–362 (2008). Medline doi:10.1038/embor.2008.28

23. M. Boissan, D. Wendum, S. Arnaud-Dabernat, A. Munier, M. Debray, I. Lascu, J. Y. Daniel, M. L. Lacombe, Increased lung metastasis in transgenic NM23-Null/SV40 mice with

hepatocellular carcinoma. *J. Natl. Cancer Inst.* **97**, 836–845 (2005). Medline doi:10.1093/jnci/dji143

24. I. Mocan, F. Georgescauld, P. Gonin, D. Thoraval, L. Cervoni, A. Giartosio, S. Dabernat-Arnaud, M. Crouzet, M. L. Lacombe, I. Lascu, Protein phosphorylation corrects the folding defect of the neuroblastoma (S120G) mutant of human nucleoside diphosphate kinase A/Nm23-H1. *Biochem. J.* **403**, 149–156 (2007). Medline doi:10.1042/BJ20061141

25. T. Ban, J. A. Heymann, Z. Song, J. E. Hinshaw, D. C. Chan, OPA1 disease alleles causing dominant optic atrophy have defects in cardiolipin-stimulated GTP hydrolysis and membrane tubulation. *Hum. Mol. Genet.* **19**, 2113–2122 (2010). Medline doi:10.1093/hmg/ddq088

26. M. Erent, P. Gonin, J. Cherfils, P. Tissier, G. Raschellà, A. Giartosio, F. Agou, C. Sarger, M. L. Lacombe, M. Konrad, I. Lascu, Structural and catalytic properties and homology modelling of the human nucleoside diphosphate kinase C, product of the DRnm23 gene. *Eur. J. Biochem.* **268**, 1972–1981 (2001). Medline doi:10.1046/j.1432-1327.2001.2076.doc.x

27. G. Montagnac, H. de Forges, E. Smythe, C. Gueudry, M. Romao, J. Salamero, P. Chavrier, Decoupling of activation and effector binding underlies ARF6 priming of fast endocytic recycling. *Curr. Biol.* **21**, 574–579 (2011). Medline doi:10.1016/j.cub.2011.02.034

28. L. Griparic, T. Kanazawa, A. M. van der Bliek, Regulation of the mitochondrial dynamin-like protein Opa1 by proteolytic cleavage. *J. Cell Biol.* **178**, 757–764 (2007). Medline doi:10.1083/jcb.200704112

29. O. Söderberg, M. Gullberg, M. Jarvius, K. Ridderstråle, K. J. Leuchowius, J. Jarvius, K. Wester, P. Hydbring, F. Bahram, L. G. Larsson, U. Landegren, Direct observation of individual endogenous protein complexes in situ by proximity ligation. *Nat. Methods* **3**, 995–1000 (2006). Medline doi:10.1038/nmeth947

30. S. Cohen, M. Megherbi, L. P. Jordheim, I. Lefebvre, C. Perigaud, C. Dumontet, J. Guitton, Simultaneous analysis of eight nucleoside triphosphates in cell lines by liquid chromatography coupled with tandem mass spectrometry. *J. Chromatogr. B Analyt. Technol. Biomed. Life Sci.* **877**, 3831–3840 (2009). Medline doi:10.1016/j.jchromb.2009.09.030

31. T. W. Traut, Physiological concentrations of purines and pyrimidines. *Mol. Cell. Biochem.* **140**, 1–22 (1994). Medline doi:10.1007/BF00928361

32. A. Quan, P. J. Robinson, Rapid purification of native dynamin I and colorimetric GTPase assay. *Methods Enzymol.* **404**, 556–569 (2005). Medline doi:10.1016/S0076-6879(05)04049-8

33. K. Takei, V. I. Slepnev, V. Haucke, P. De Camilli, Functional partnership between amphiphysin and dynamin in clathrin-mediated endocytosis. *Nat. Cell Biol.* **1**, 33–39 (1999). Medline